




Modeling of the curing kinetics of acrylate photopolymers for additive manufacturing

Robert Setter^{1,2}  | Stefan Schmörlzer³ | Natalie Rudolph³  |
Elena Moukhina³ | Katrin Wudy^{1,2} 

¹Professorship of Laser-based Additive Manufacturing, Department of Mechanical Engineering, TUM School of Engineering & Design, Technical University of Munich, Garching, Germany

²Collaborative Research Center 814 (CRC 814), Friedrich-Alexander University Erlangen-Nuremberg, Erlangen, Germany

³NETZSCH-Gerätebau GmbH, Selb, Bayern, Germany

Correspondence

Robert Setter, Professorship of Laser-based Additive Manufacturing, Department of Mechanical Engineering, TUM School of Engineering & Design, Technical University of Munich, Boltzmannstr. 15, 85748 Garching, Germany.

Email: robert.setter@tum.de

Funding information

Deutsche Forschungsgemeinschaft, Grant/Award Number: Project-ID. 61375930

Abstract

Next-generation additive manufacturing (AM) processes such as multiphoton lithography and the fusion jetting (FJ) process demonstrate increasing demands toward temperature stability and a thoroughly understood curing behavior of acrylate photopolymers. This investigation targets the utilization of different kinetic models based on experimentally determined calorimetric results of different acrylate systems. The goal is to determine a holistic model that successfully describes the simultaneous dependency of the curing behavior on the temperature and the UV intensity. Two consecutive modeling strategies are investigated: a single measurement analysis followed by a clustered measurement analysis. In both cases, models based on the Kamal–Sourour method provide superior coefficients of determination above 0.99. First conclusions were drawn toward selected kinetic parameters, such as the temperature independence of the respective reaction orders. The model was then successfully utilized for first predictions of the curing behavior, demonstrating plausible progressions of the degree of cure for not experimentally determined UV intensities.

KEYWORDS

additive manufacturing, degree of polymerization, differential scanning calorimetry, kinetics (polym.), photopolymerization

1 | MOTIVATION

Next-generation additive manufacturing (AM) processes based on UV curing of acrylate photopolymers combine rapid processing speeds, complex geometries with high resolutions, and an extended material spectrum for multimaterial part production. This contains processes such as multiphoton lithography, as well as the experimental fusion jetting (FJ) technology for multimaterial polymer parts.¹ FJ introduces acrylate-based photopolymers to the

high-temperature environment of laser-based powder bed fusion of plastics (PBF-LB/P).^{2,3} Compared with state-of-the-art photopolymer-based AM, the temperature experienced by the acrylate during processing represents a critical factor regarding the curing behavior for both technologies. The temperature along with the UV intensity can be utilized to increase or decrease the extent and speed of the curing reaction of the photopolymer, which was demonstrated experimentally in Reference [4]. Further, high temperatures proved challenging for the

This is an open access article under the terms of the [Creative Commons Attribution](https://creativecommons.org/licenses/by/4.0/) License, which permits use, distribution and reproduction in any medium, provided the original work is properly cited.

© 2023 The Authors. *Polymer Engineering & Science* published by Wiley Periodicals LLC on behalf of Society of Plastics Engineers.

thermal stability of specific components of the examined acrylate systems. Besides the experimental analysis of acrylate-based photopolymers, the mathematical description of the reaction mechanisms represents an essential cornerstone for process understanding and future optimizations. The mathematical models to describe the curing kinetics of acrylate systems for the abovementioned technologies should consider the temperature and the UV intensity collectively. Similar holistic kinetic approaches are investigated in comparable fields, for example, by Bloh,⁵ who describes the combined influence of temperature and UV intensity on the kinetics of photocatalytic reactions. However, within the field of photopolymer-based AM, most kinetic modeling attempts are restricted to the variation of the temperature or the UV intensity solely. For example, Redmann et al.⁶ utilize a model-free approach for describing the curing kinetics of the secondary heat treatment of a calorimetrically analyzed epoxy-based b-stage photopolymer. A similar approach is presented by Konuray et al.⁷ focusing on a model-based approach represented by the Kissinger–Akahira–Sunose method. In multiphoton lithography, the curing kinetics of the thermal post-cure of acrylate-based photopolymers has been investigated by Bauer⁸ based on experimentally gathered data through Raman spectroscopy. Taki et al.⁹ numerically simulated photopolymerization kinetics based on the UV intensity with the addition of the oxygen-based diffusion behavior during vat photopolymerization processing. Kim et al.¹⁰ describe the temperature dependence of the curing kinetics of photopolymers between -10 and 70°C for a constant UV intensity. The utilized model describes an autocatalytic reaction mechanism and is based on data gathered through differential scanning calorimetry with a UV-light source (UV-DSC). Also, Bachmann et al.¹¹ previously demonstrated the validity of UV-DSC to successfully describe the curing kinetics of photopolymer systems.

This investigation introduces and evaluates complementary kinetic models to describe the curing reactions of acrylate-based photopolymers for next-generation AM technologies, which consider the UV intensity and the process temperature similarly. Compared with conventional UV-curable systems such as epoxy-based adhesives, acrylate systems demonstrate faster curing times within seconds.^{12,13} Fast curing times represent a fundamental requirement for the reduction of layer time for future AM processing of volatile substances at elevated temperatures. The goal of the investigation is to identify models that combine the high coefficients of determination for a valid depiction of the curing kinetics with sufficient informational output toward the chemical reactions. For this, different kinetic models are established and

evaluated regarding their degree of determination and chemical plausibility to describe the degree of cure and the reaction rate. Important kinetic factors such as the reaction rate constant k are investigated as functions f dependent on the temperature T and the UV intensity I : $k=f(I, T)$. The models are fitted toward experimentally determined UV-DSC data points. All experimental results were gathered and discussed in Reference [4]. The curve-fitting procedures follow two different approaches: single measurement analysis and clustered measurement analysis. Based on the results, first predictions for nonmeasured parameter sets are performed. The ability to predict the curing behavior represents a promising tool for future optimization of the process parameters of AM processing in a high-temperature environment. The predictions facilitate the non-experimental determination of process parameter sets to achieve a specific degree of cure while considering the limitation of the temperature exposure and thermal decomposition of the acrylate system. Therefore, elevated final part qualities can be achieved.

2 | THEORETICAL BASICS: KINETIC MODELING

2.1 | Conversion rate

To describe the conversion achieved during curing reactions, the so-called degree of cure is calculated as follows¹⁴:

$$\alpha = \frac{\Delta H}{H_{total}} = \frac{\int_{t_{start}}^t \dot{Q} dt}{H_{total}} \quad (1)$$

In this, the achieved conversion α is the ratio between the partially emitted exothermic amount of specific energy ΔH and the total amount of reaction enthalpy available H_{total} . In the case of DSC or UV-DSC, ΔH is described as the integral of the specific heat flow \dot{Q} over time t from the start of the reaction t_{start} . The conversion rate $\frac{d\alpha}{dt}$ is the time-dependent derivative of the conversion α . One of the most important equations in reaction kinetics for describing $\frac{d\alpha}{dt}$ is represented through the following ordinary differential equation¹⁵:

$$\frac{d\alpha}{dt} = k \cdot f(\alpha) \quad (2)$$

Equation (2) introduces two values: the reaction mechanism $f(\alpha)$ dependent on the reaction type and the reaction rate constant k . In case of a solely thermally

controlled reaction, k is dependent on the isothermal temperature T applied during curing. This can be described by the Arrhenius equation¹⁶:

$$k(T) = A \cdot e^{-E_a/RT} \quad (3)$$

The activation energy E_a is a value correspondent to the magnitude of the energy barrier to reaction, while $R = 8.314 \text{ J/mol K}$ is the universal gas constant and A the pre-exponential factor or frequency factor.¹⁵ Dependent on the reaction mechanism, different mathematical models can be used to either directly describe α or the acceleratory function $\frac{d\alpha}{dt}$. With those models, different reaction-specific kinetic values such as the reaction order n are introduced. The values are either constant or can be correlated to specific variable process parameters. In the following, the reaction models and reaction mechanisms $f(\alpha)$ (compare Equation (2)) relevant for this investigation are described in detail.

2.2 | The Avrami equation

A simplified and nondifferential approach to describe the reaction kinetics of a sigmoidal progression of the conversion α is the so-called Avrami method.¹⁷ In this, α is dependent on the reaction rate constant k_A , the reaction time t , and the reaction order n_A :

$$\alpha(t) = 1 - e^{-k_A \cdot t^{n_A}} \quad (4)$$

The Avrami equation is originally intended to describe the phase transition for characteristically sigmoidal-shaped transformation curves. This is the case, for example, for the crystal growth in semi-crystalline thermoplastics. Investigations by Jiang et al.¹³ Murias et al.¹⁸ and Xu et al.¹⁹ showed that the UV-curing reactions of photopolymers achieve promising fits for this approach. For all investigations, the general assumption was made that the phase change from liquid to solid can be described through the Avrami equation. For an acrylic photopolymer, Jiang et al. pointed out a linear correlation of the UV intensity with the reaction rate constant k_A as well as the reaction order n_A . Considering the Avrami equation for the description of UV-curing reactions takes into account the general simplification, that the sigmoidal-shaped curve needs to have a symmetrical progression. This is often not the case for real-life UV-curing reactions and eventually leads to a challenging depiction of the start and end of the reaction

as well as for accelerating mechanisms and different reaction paths. Nevertheless, depicting the reaction behavior of the UV-curing reactions with the Avrami equation is still examined for this investigation because of its advantageous simplicity and mathematical definiteness compared with most of the kinetic models examined in this investigation. As mentioned before, the Avrami method is originally intended for heterogenous reaction mechanisms such as crystal growth in a thermoplastic polymer. Heterogenous in this context means that chemically identical constituents of the reactant may possess different reactivities depending upon their location within the sample and the history of each sample preparation.¹⁵ This is contrary to homogenous reaction mechanisms, which are measurements of changes in concentration of one (or more) reactants or products with time, at constant temperature.¹⁵ In a homogenous case, the reaction rate can be described using previously discussed Equation (2) (compare 2.1) with the respective reaction mechanism $f(\alpha)$. In case of polymer-based curing, there are two important models to mathematically describe $f(\alpha)$: the n -th order reaction model and the autocatalytic reaction model. Both are introduced in the following.

2.3 | N-th order reaction model

The widely used Freeman and Carroll method²⁰ or n -th order reaction model represents a homogenous reaction mechanism $f(\alpha)$ (compare 2.1, Equation (2)) based on the consumption of reactant molecules. It is dependent on the conversion α and the reaction order n_{nth} :

$$f(\alpha) = (1 - \alpha)^{n_{nth}} \quad (5)$$

Based on Equation (5), a reaction order of $1 < n_{nth} < 3$ usually indicates a purely homogenous chemical reaction. Further, an ideal first-order reaction ($n_{nth} = 1$) can, for example, indicate molecular structural rearrangements.¹⁵ $n_{nth} < 1$ or $n_{nth} > 3$ can be an indication of non-chemical or inhomogeneous reactions. The consumption of reactant molecules of the n -th order reaction is correlated to the initial maximum in exothermal heat dissipated, followed by a continuous decline of reactivity with progressing cross-linking of the polymer. Besides representing an advantageously simple approach, different investigations indicate alternative models or extensions of Equation (5) to realistically describe the reaction kinetics of polymer cross-linking.²¹⁻²³ In the following, the so-called autocatalytic reaction model is introduced.

2.4 | Autocatalytic reaction model

Another reaction mechanism is the autocatalytic reaction model or Sestàtk–Berggren model.²⁴ In this case, the reaction mechanism $f(\alpha)$ is calculated as follows:

$$f(\alpha) = \alpha^m (1 - \alpha)^n \quad (6)$$

The autocatalytic reaction model is intended for the representation of cross-linking and polymerization reactions, with n and m representing the autocatalytic reaction order. Contrary to the n -th order reaction, the autocatalytic reaction is a self-accelerating reaction, which starts with a minimum of exothermal heat dissipated. After that, the heat flow increases until a global maximum is reached. Finally, the heat flow symmetrically declines until the reaction is over. The simplest form of the autocatalytic reaction model is the Prout–Tompkins equation ($n = m = 1$)²⁵:

$$f(\alpha) = \alpha(1 - \alpha) \quad (7)$$

Similar to the Avrami model and the n -th order reaction (compare 2.2 and 2.3), the autocatalytic reaction has limitations to fully function as an ideal representation of cross-linking reactions. Du et al.²⁶ Zhuqing et al.,²⁷ and Raja Pandiyan et al.²⁸ attempted kinetic modeling of epoxy resins and polyester resins respectively with the Sestàtk–Berggren model. In all cases, the curve fits showed challenging behavior capturing all segments of the reaction equally. The deviations are particularly present at the start/end of the reaction. As a modification, Raja Pandiyan et al. successfully introduced a diffusion factor to achieve a more tailored representation. Galukhin et al.²⁹ also introduced a diffusion-based kinetic model for thermal curing of an adamantane-based dicyanate ester. The model complements the initial curing reaction with a diffusion factor f_d , which considers the conversion α as well as the final conversion of the polymer. The implementation of diffusion factors was also considered for this investigation. However, the results showed a reduction in the fit quality of the mathematical functions compared with sole reaction-driven kinetic models. A reason for this behavior is represented by the short reaction time as well as the distinction of the photopolymer curing reaction from a sole temperature-dependent curing reaction. Therefore, diffusion-driven models are not further discussed in this investigation. Instead, an alternative approach is represented by the consideration of parallel and complementary reaction pathways. This can be achieved through combination of

the n -th order and autocatalytic reaction models and will be explained in the following.

2.5 | Combined n -th order and autocatalytic reaction model: The Kamal–Sourour equation

The n -th order reaction model and the autocatalysis reaction model are characterized by individual reaction pathways: $A \rightarrow B$ (n -th order) and $A + B \rightarrow 2B$ (autocatalytic). Through combination of both methods, the n -th order reaction becomes a complementary asset to the autocatalytic reaction and acts as a necessary initiating feature by providing its product B as an educt for the autocatalysis. This correlation can be represented through the Kamal–Sourour equation,³⁰ which proved as an adequate description of thermoset curing, especially for thermally cured epoxy systems:

$$\frac{d\alpha}{dt} = k_1 \cdot (1 - \alpha)^{n_{gen}} + K_{cat,gen} * k_2 \cdot \alpha^{m_{gen}} (1 - \alpha)^{n_{gen}} \quad (8)$$

In its general form, the Kamal–Sourour equation is a combination of Equations (2), (5), and (6) with the optional addition of a weight factor $K_{cat,gen}$ to represent the contribution of the autocatalysis reaction.³¹ m_{gen} and n_{gen} are the temperature-independent reaction orders of the autocatalytic and n -th order reaction respectively, while k_1 and k_2 are the reaction rate constants of each path. Multiple investigations demonstrate a sufficient representation of thermoset curing kinetics with the general Kamal–Sourour equation. Other investigations demonstrate modified versions of the Kamal–Sourour equation by considering a shared reaction rate constant for both pathways³² or individual reaction orders n_1 and n_2 for n -th order and autocatalysis reactions respectively.³³ For this investigation, the Kamal–Sourour model is examined for kinetic modeling in its general form only (Equation 8).

3 | MATERIALS AND METHODS

3.1 | Materials

The materials used for this investigation are UV DLP Firm and UV DLP Hard by the company photocentric 3D. Both reactive liquids are photopolymers with diacrylates and dimethacrylates as their proprietary building elements.^{34,35} The materials are selected due to their profound mechanical properties after cross-linking, fast

curing speeds, and sufficient controllability of the viscosity behavior through temperature increase, which has been described in previous investigations.² Combined with thermoplastic elastomeric powders, both acrylates represent promising partners for future hard-soft structures and selective reinforcements created through the FJ process. For simplification and better representation in diagrams and tables, the respective materials are abbreviated as “Acrylate A” and “Acrylate B” throughout this investigation. The chemical structures of the diacrylates and dimethacrylates can be found in Figure 1A. Potential interaction points for polymer chain formation are highlighted with arrows. These interaction points correlate to all present C=C double bonds within the monomer structure of the diacrylates and dimethacrylate, which represent the starting points of most photopolymerization reaction pathways.³⁶ The substituent groups *R* are also considered as starting points since there is only restricted information about the content of double bonds within the entirety of the molecular structure.

3.2 | Differential scanning calorimetry measurements with a UV-light source

The kinetic models of this investigation are based on results from differential scanning calorimetry measurements with a UV-light source (UV-DSC). A detailed description of the experimental setup as well as a detailed analysis of the measurement results can be found in Reference [4]. The experiment parameters are summarized in Table 1. The UV-DSC measurements were performed with UV intensities of 7.5, 15, 30, and 60 mW/cm² at isothermal temperatures of 30, 90, and 150°C. The UV treatments are performed twice for 10 min. Through curve subtraction, a horizontal baseline is created and complete curing is verified. Before UV-light activation, soak times of 10 min are included. Heating rate is 5 K/min and the cooling rate of 20 K/min is used with a five-second delay before the UV treatment.⁴

TABLE 1 Summarized experimental parameters for UV-DSC measurements of Acrylate A and Acrylate B liquid samples as described in Reference [4].

Isothermal temperatures/°C	30, 90, 150
Soak time t_{soak} /min	10
Heating rate/K/min	5
Cooling rate/K/min	20
UV intensities/mW/cm ²	7.5, 15, 30, 60
Radiation time/min	10
Delay before irradiation start in s	5

3.3 | Modeling approach

The modeling approach of this investigation is divided into two consecutive procedures: single measurement analysis and clustered measurement analysis. The single measurement analysis is utilized as pre-selection criteria for identification of the most relevant kinetic model to describe the experimental UV-DSC data. The consecutive clustered procedure is then performed based on the lessons learned from the single measurement analysis for a selected kinetic model with the highest coefficient of determination. Except reaction orders, the interpretation of the kinetic parameters is primarily performed qualitatively and not quantitatively for both procedures. The single measurement analysis is performed as follows:

1. Automated curve fitting of the respective kinetic model with the achieved conversion α based on the experimentally gathered UV-DSC data.
2. Evaluation of the fit accuracy based on the coefficient of determination R^2 .
3. Analysis of the correlation between the respective kinetic values and the isothermal temperature during curing as well as the UV intensity.
4. Discussion and evaluation of the results toward their physical and chemical plausibility.

For the single measurement analysis, all curve-fitting procedures of all nondifferential equations (such as the Avrami method) are performed using the Levenberg–Marquardt algorithm³⁷ with a maximum number of 500 iterations. In the case of all ordinary differential equations (compare Equation (2)), the Runge–Kutta method RK 45³⁸ is applied, also with a maximum number of 500 iterations.

According to the recommendations developed by the Kinetics Committee of the International Confederation for Thermal Analysis and Calorimetry (ICTAC),³¹ a clustered analysis of multiple measurements for different heating rates and/or isothermal temperatures is advisable to guarantee valid results for kinetic modeling. This includes a substitution of the reaction rate constant with a more detailed mathematical model. For thermally triggered curing reactions, this can be achieved by substituting $k(T)$ with the Arrhenius equation (compare Equation (3)). However, since the curing reactions of this investigation are triggered by photon interaction and not by temperature increase, the activation energy can technically not be considered as an energy threshold provided by temperature increase.⁴ Accordingly, instead of an Arrhenius-based reaction rate constant $k(T)$ (compare Equation (3)), a substituted version of an Arrhenius-like exponential decay function is

used to describe the reaction rate constant $k(I, T)$ in dependence of the UV intensity I and the temperature T . The clustering can be performed in two ways for $k(I, T)$, which are summarized in Table 2. In case of clustering regarding the UV intensity, $k(I, T)$ can be described by Equation (9):

$$k(I, T) = A(I) \cdot e^{-D(I)/T} \quad (9)$$

In case of clustering regarding the temperature, $k(I, T)$ can be described by Equation (10):

$$k(I, T) = A(T) \cdot e^{-D(T)/I} \quad (10)$$

For both Equations (9) and (10), D and A are referred to as exponential factor and pre-exponential factor, respectively, throughout this investigation. The kinetic modeling procedure for clustered measurement analysis

follows the same pattern as represented by steps (1)–(4) of the kinetic modeling procedures for single measurements described above. For all clustered calculations, a commercial software (Kinetics Neo, NETZSCH GmbH, Germany) is used, which is mathematically based on the Euler method.

4 | RESULTS AND DISCUSSION

4.1 | Overall comparison of different kinetic models based on single measurements

Figure 1B depicts all models discussed before, which are exemplarily fitted to the UV-DSC data of Acrylate A for a UV intensity of 7.5 mW/cm^2 at 30°C . For better representation of the quality of each fit, only the first 50 s of the reaction is shown. Besides only depicting one measurement, the following conclusions can be considered as

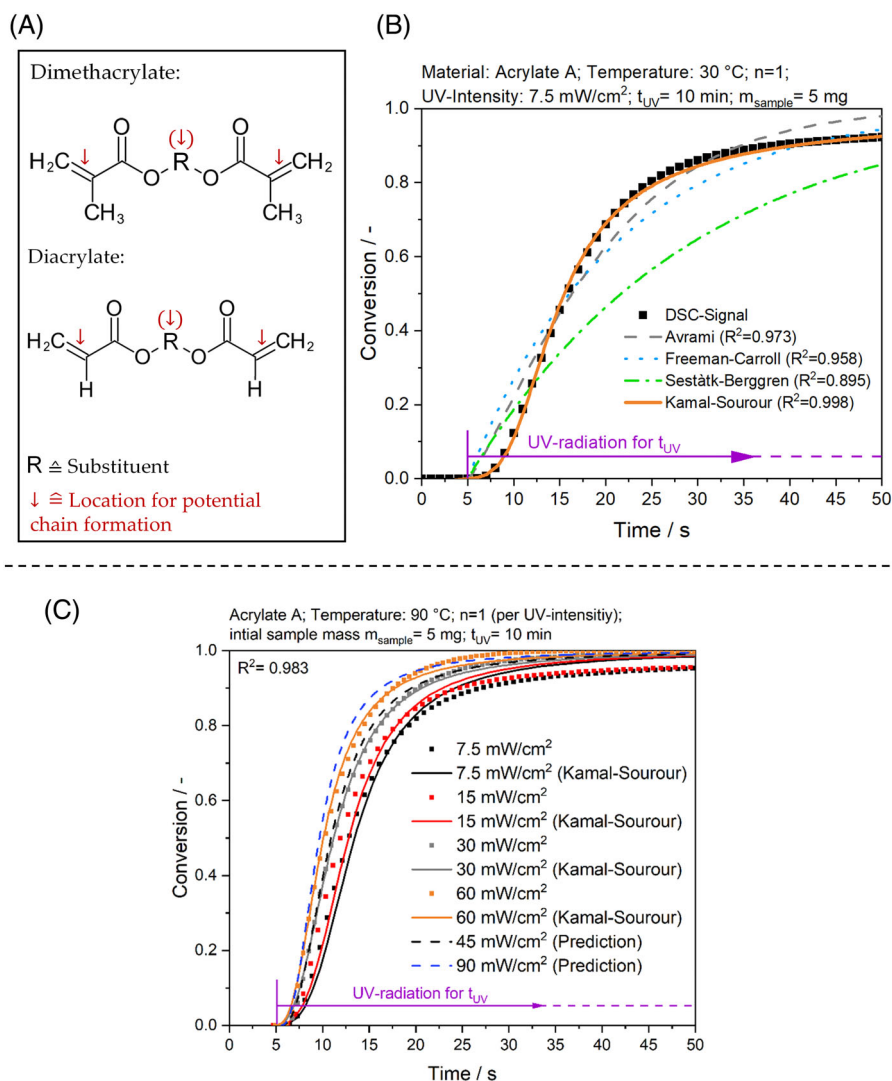
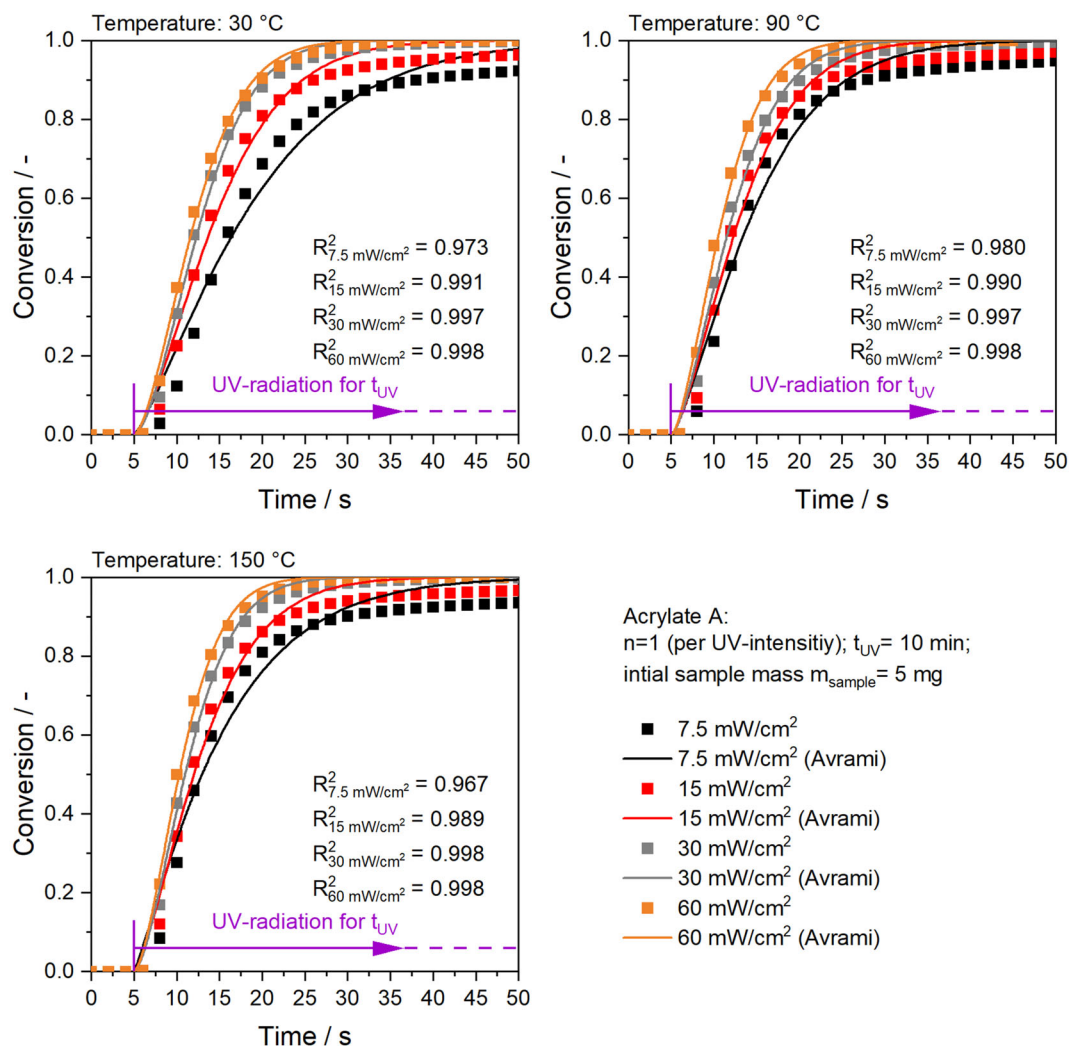


FIGURE 1 (A) Dimethacrylates and diacrylates as proprietary building elements for Acrylate A and Acrylate B; (B) Exemplary curve-fitting results of different kinetic models (including their coefficient of determination R^2) for description of the curing reaction of Acrylate A for a UV intensity of 7.5 mW/cm^2 at an isothermal temperature of 30°C ; (C) Kinetic predictions for Acrylate A at 90°C for UV intensities of 40 and 90 mW/cm^2 based on the enhanced Kamal-Sourour equation (compare Equation (12)) in comparison with originally measured UV-DSC data.

TABLE 2 Clustering methods for kinetic analysis of Acrylate A and B based on UV intensity and temperature.

UV-intensity-based clustering of UV-DSC measurements		Temperature-based clustering of UV-DSC measurements	
Cluster 1: 7.5 mW/cm ²	30, 90, 150°C	Cluster 1:	7.5, 15, 30, 60 mW/cm ² 30°C
Cluster 2: 15 mW/cm ²	30, 90, 150°C	Cluster 2:	7.5, 15, 30, 60 mW/cm ² 90°C
Cluster 3: 30 mW/cm ²	30, 90, 150°C	Cluster 3:	7.5, 15, 30, 60 mW/cm ² 150°C
Cluster 4: 60 mW/cm ²	30, 90, 150°C		

FIGURE 2 Single measurement analysis of Acrylate A with the Avrami method for UV intensities 7.5, 15, 30, and 60 mW/cm² as well as temperatures of 30, 90, and 150°C.

generally applicable for all measurements and materials analyzed.

The achieved results vary strongly based on the method and the individual variations of each method implemented. With a coefficient of determination R^2 of 0.895, the Seståtk–Berggren model represents the worst fit of all successfully converged models, followed by the

Freeman–Carroll method with an R^2 of 0.958. A single n -th order or autocatalytic reaction mechanism for the description of the reaction behavior of both materials is therefore not advisable. The Avrami method shows the second best fit of all depicted kinetic models with an R^2 of 0.973. The best fit of all kinetic models examined is the Kamal–Sourour equation for both materials analyzed. In

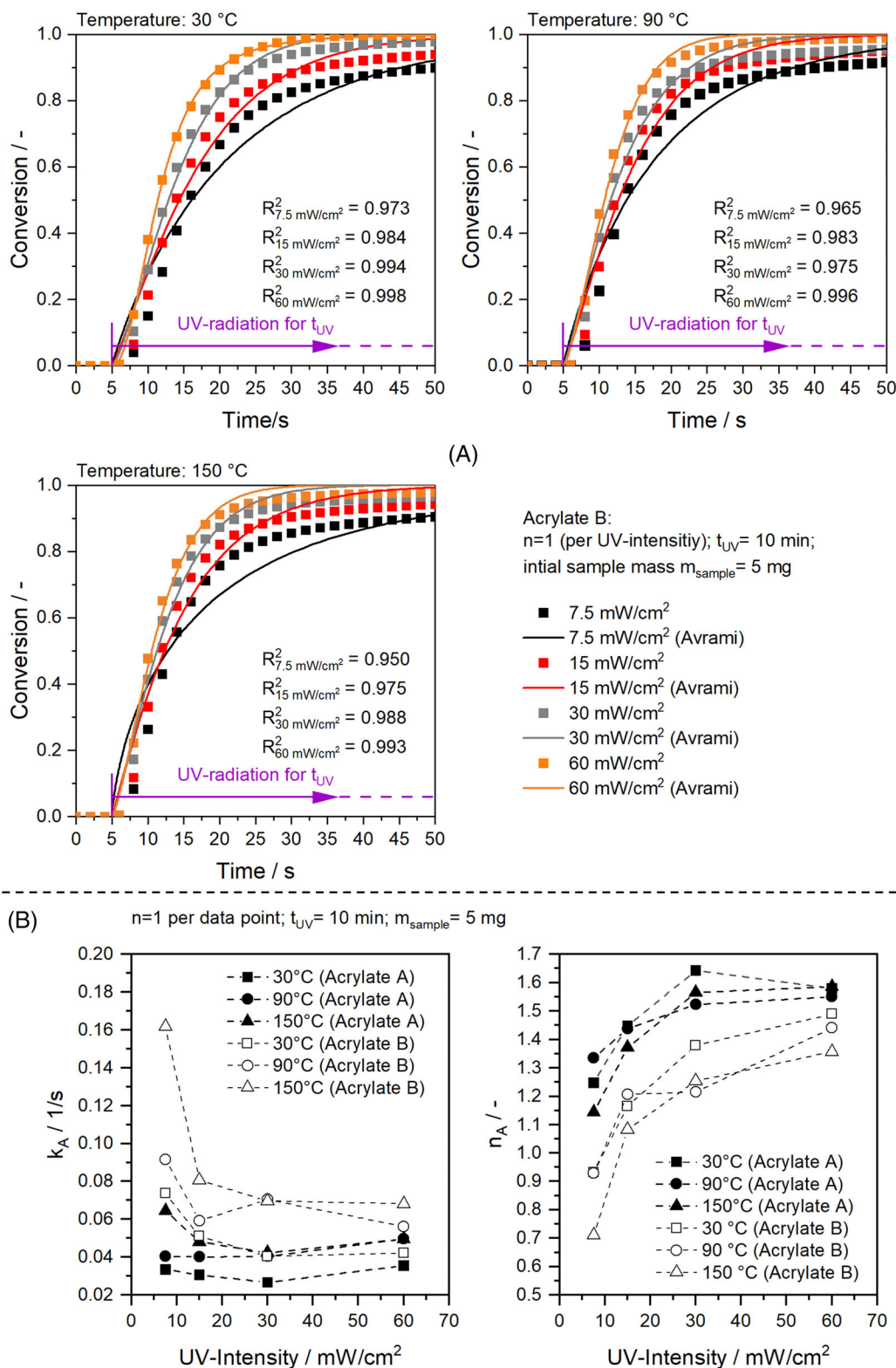


FIGURE 3 (A) Single measurement analysis of Acrylate B with the Avrami method for UV intensities 7.5, 15, 30, and 60 mW/cm² as well as temperatures of 30, 90, and 150 °C; (B) Dependency of the reaction rate constant k_A and the reaction order n_A from the UV intensity at different isothermal temperatures for Acrylate A and Acrylate B based on the Avrami method (compare Equation (4)).

the example presented in Figure 1A, the Kamal–Sourour equation reaches an R^2 of 0.998. The only model not implemented is the Prout–Tompkins method, for which

it is not possible to create a converging fit to the UV-DSC data due to limited modifiability of the mathematical model. In the following, the results of the Avrami method

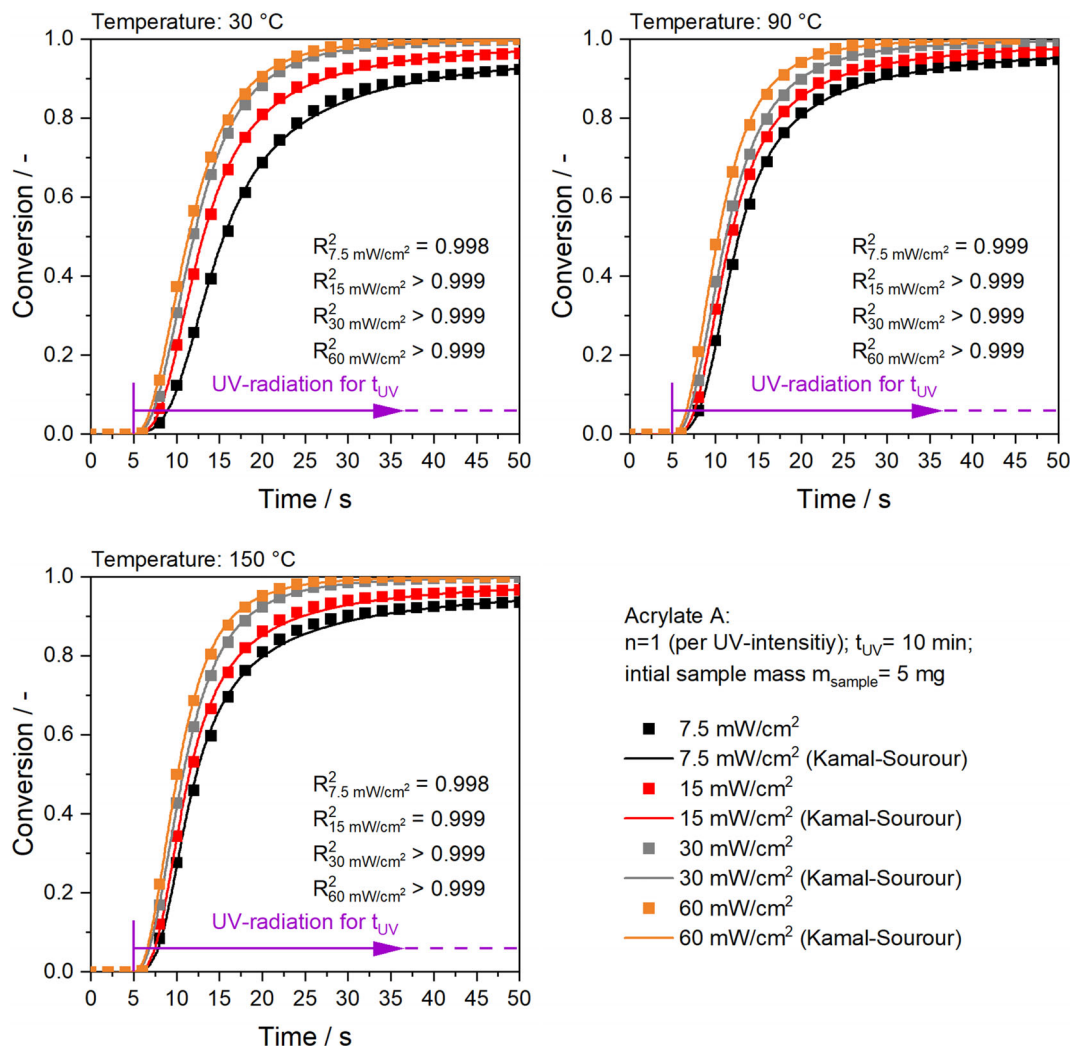


FIGURE 4 Single measurement analysis of Acrylate A with the Kamal-Sourour method (compare Equation (8)) for UV intensities 7.5, 15, 30, and 60 mW/cm² as well as temperatures of 30, 90, and 150 °C.

(compare 2.2) as well as of the general Kamal-Sourour equation (compare 2.5) are presented in detail.

Figures 2, 3A show the curve-fitting results with the Avrami equation for Acrylate A and Acrylate B, respectively. As can be seen, coefficients of determination R^2 can be achieved between 0.973 and 0.998 for Acrylate A as well as 0.950 and 0.998 for Acrylate B. An increase of R^2 with increasing UV intensities is visible for both materials.

As discussed in Section 2.2, the Avrami equation is dependent on two parameters: the reaction rate constant k_A and the reaction order n_A . Their dependencies of the UV intensity and isothermal temperature for Acrylate A are depicted in Figure 3B. With increasing temperature, the results for k_A achieve higher values globally compared with lower temperatures. For Acrylate A, the values vary between 0.025 and 0.035 s⁻¹ for 30 °C, between 0.04 and 0.05 s⁻¹ for 90 °C, and between 0.0425

and 0.065 s⁻¹ for 150 °C. The results of Acrylate B show similar behavior for increasing temperatures, with a generally higher magnitude achieved in k_A values up to 0.162 s⁻¹ at 150 °C. A potential hypothesis for the global increase of the k_A values with increasing temperatures is represented through the collision theory proposed by Trautz³⁹ and Lewis⁴⁰ since k_A is directly proportional to the reaction rate. A clear correlation to the UV intensity with the reaction rate constant k_A cannot be detected due to varying progression of the individual curves for both materials. Contrary to the behavior of the reaction rate constant k_A described above, the reaction order n_A presented in Figure 3 shows a distinct increase with increasing UV intensities for all isothermal temperatures analyzed. For Acrylate A, the values for the reaction order n_A are located between 1.25 and 1.35 for 7.5 mW/cm², 1.35 and 1.45 for 15 mW/cm², 1.5 and 1.65 for 30 mW/cm², and 1.5 and 1.6 for 60 mW/cm². Slightly

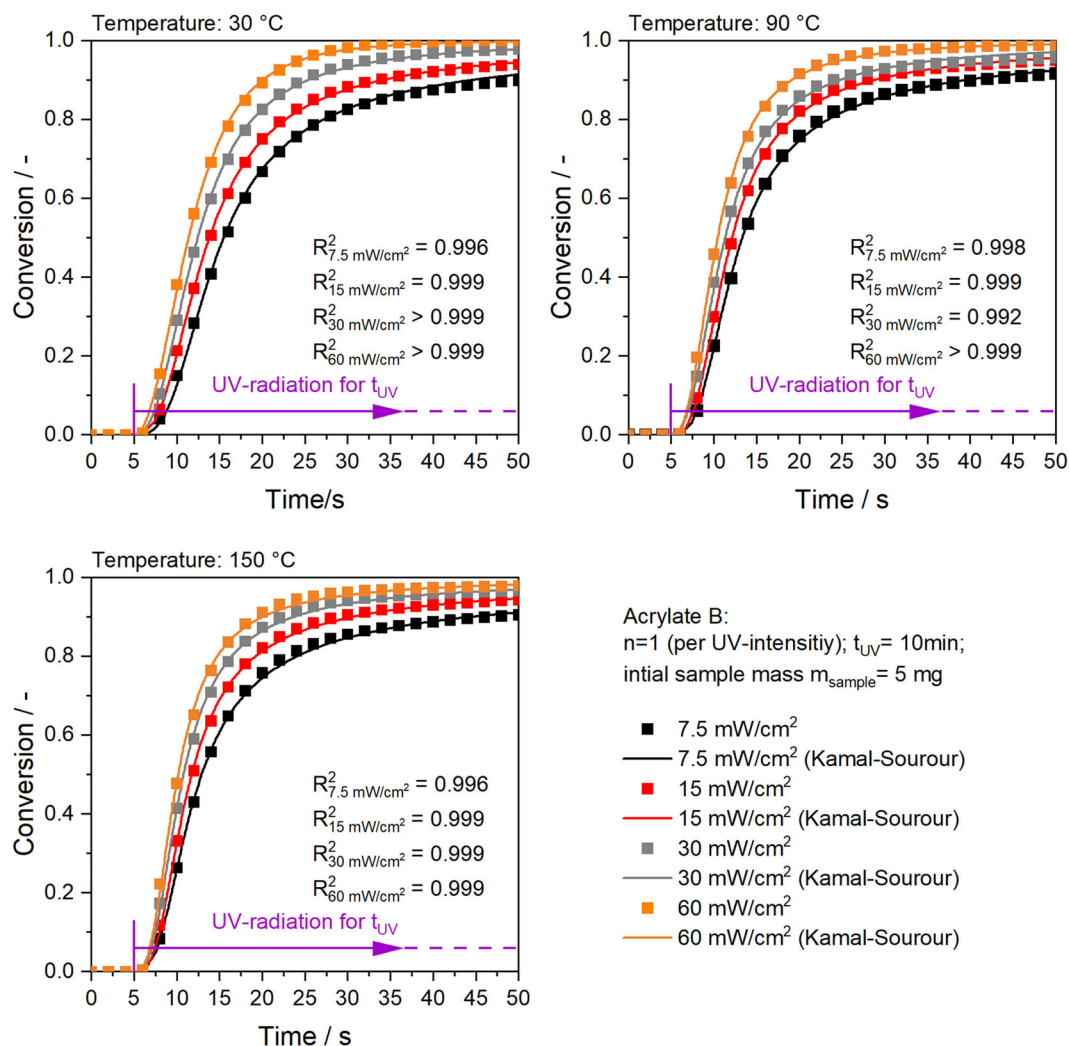


FIGURE 5 Single measurement analysis of Acrylate B with the Kamal-Sourour method for UV intensities 7.5, 15, 30, and 60 mW/cm² as well as temperatures of 30, 90, and 150 °C.

lower values between 0.93 and 1.37 are achieved for Acrylate B. The progression of all curves indicates a limited growth function with a saturation limit for UV intensities above 30 mW/cm². This is contrary to the investigations by Jinag et al.¹³ which point out a linear increase of reaction order n_A in the depicted UV-intensity spectrum of the investigation. For different temperatures, nearly identical n_A values can be partially detected for Acrylate A and Acrylate B. In the case of the temperature, no clear correlation with the reaction order n_A can be derived from the results presented.

Figures 4, 5 show the curve-fitting results with the general Kamal-Sourour method for Acrylate A and Acrylate B, respectively, compared with the measured UV-DSC data. As can be seen, coefficients of determination R^2 can be achieved between 0.998 and above 0.999 for Acrylate A as well as 0.992 and above 0.999 for Acrylate B. A slight increase in R^2 with increasing UV

intensities is visible for both materials, identical to the Avrami method.

The general Kamal-Sourour equation is dependent on five parameters (compare 2.5): The individual reaction rate constants k_1 and k_2 , the reaction orders n_{gen} and m_{gen} , and the weight factor $K_{cat,gen}$ represent the contribution of the autocatalysis reaction. Their dependencies of the UV intensity and isothermal temperature for Acrylate A are depicted in Figure 6. Due to their multiplicative connection and interchangeability (compare Equation (8)), the values of the autocatalytic kinetic parameters k_2 and $K_{cat,gen}$ are presented in product form: $k_2 \cdot K_{cat,gen}$. As can be seen, the spectrum of the parameter values of k_1 is broad with relatively small values compared with the reaction rate constant determined with the Avrami method. A logarithmic representation of k_1 is chosen for better visualization. The k_1 values spread within a magnitude of approximately 10^{-3} and 10^{-7} for

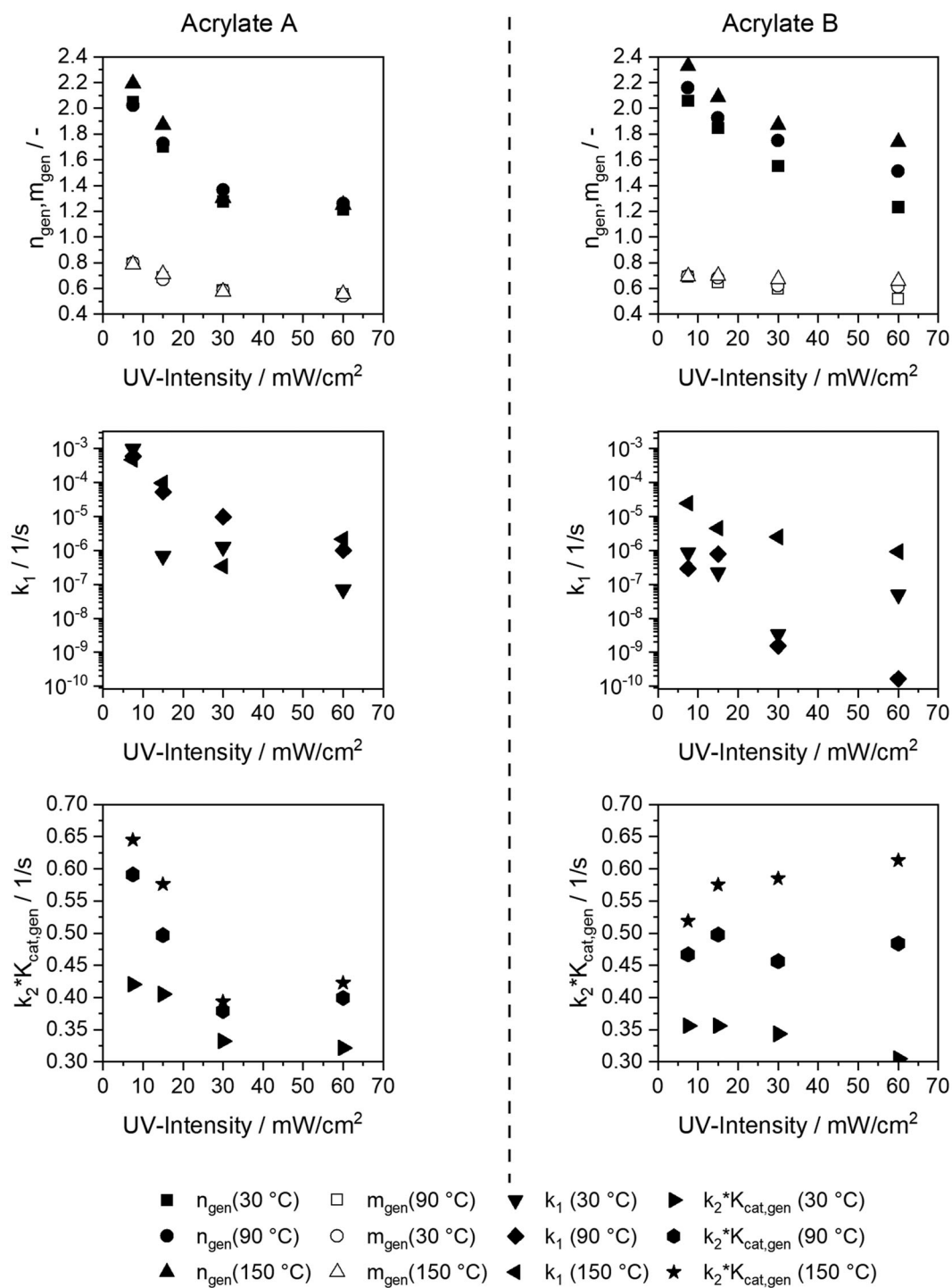


FIGURE 6 Dependency of the reaction orders n_{gen} and m_{gen} , the reaction rate constant k_1 as well as the product of the reaction rate constant and the autocatalytic pre-exponential factor $k_2 \cdot K_{cat,gen}$ from the UV intensity at different isothermal temperatures for Acrylate A and Acrylate B based on the Kamal–Sourour method (compare Equation (8)).

Acrylate A. For Acrylate B, the spread is larger with a generally smaller magnitude of the values for k_1 between 10^{-6} and 10^{-10} . The $k_2 \cdot K_{cat,gen}$ values are higher compared with the k_1 values for Acrylate A and Acrylate B, approximately achieving values between 0.32 and 0.66 s^{-1} as well as 0.30 and 0.62 s^{-1} . This difference in

magnitude can most likely be explained by the inclusion of the weight factor $K_{cat,gen}$. For Acrylate A, increase in UV intensities causes a general decrease of k_1 and $k_2 \cdot K_{cat,gen}$. The progressions of the curves are reminiscent of exponential decay functions with a saturation limit above 30 mW/cm^2 . For Acrylate B, the UV-intensity

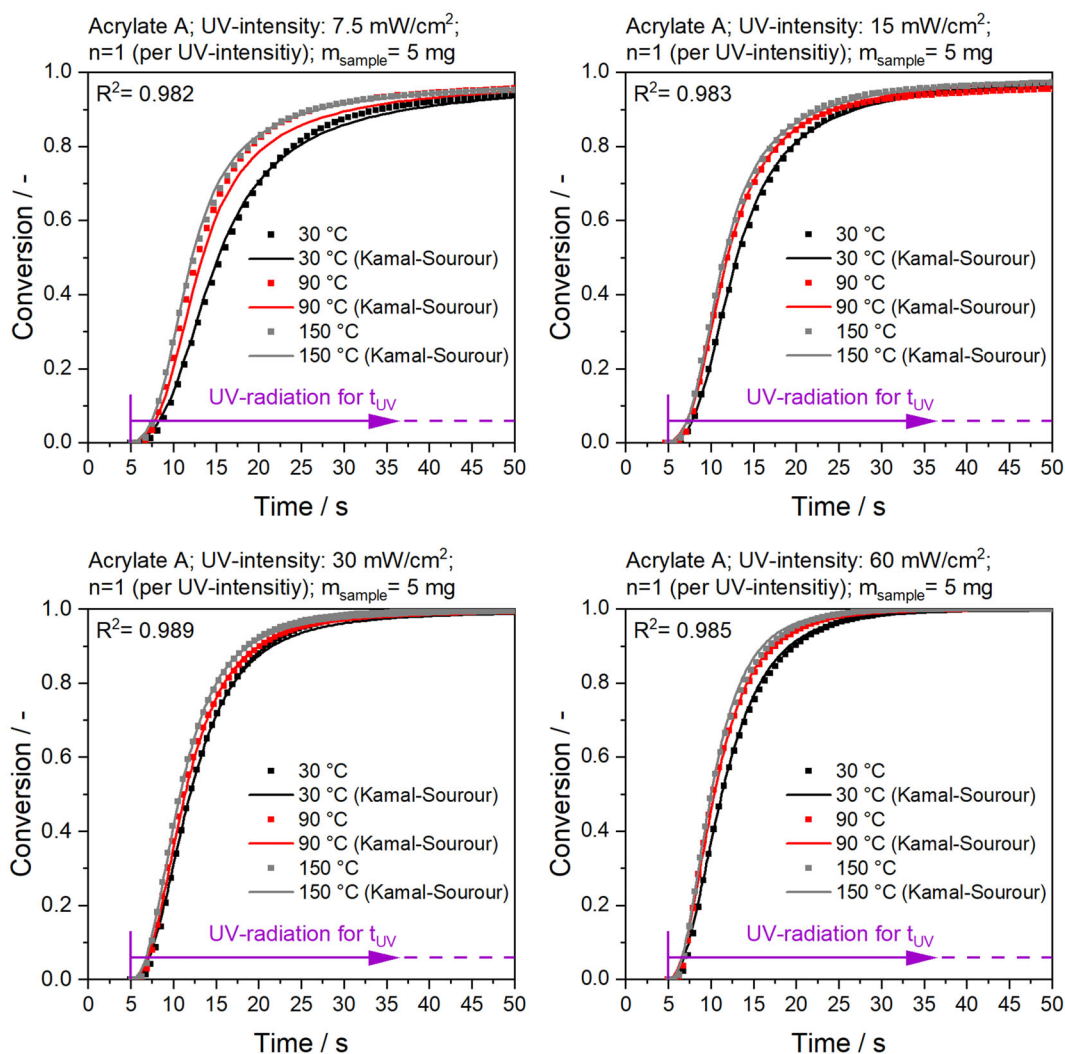


FIGURE 7 Clustered measurement analysis based on the Kamal–Sourour method described by Equation (11) of Acrylate A with an extended Kamal–Sourour method for UV intensities 7.5, 15, 30, and 60 mW/cm² as well as temperatures of 30, 90, and 150 °C.

dependent progressions of k_1 and $k_2 \cdot K_{cat,gen}$ are strongly fluctuant with the different trends for every isothermal temperature. This hinders the determination of distinct trends based on the UV intensity of this material. For both materials, the magnitude of $k_2 \cdot K_{cat,gen}$ is significantly dependent on the isothermal temperature chosen, achieving globally higher values with increasing temperatures. For the k_1 values of Acrylate B, this is valid as well. For Acrylate A however, the temperature dependency toward k_1 is ambiguous, showing either increasing, decreasing, or fluctuating values for the individual UV intensities. In this case, the highest similarity in the progression of k_1 can be seen for UV intensities of 15 and 60 mW/cm². Both experience an increase in k_1 with increasing temperatures. Compared with the results of k_1 and $k_2 \cdot K_{cat,gen}$, the reaction orders achieve results of increased precision for Acrylate A and Acrylate B with a

high definiteness for all UV intensities and temperatures. With increasing UV intensities, both reaction orders show distinct decays, which can be interpreted as exponential decay functions with visible saturation limits at $n_{gen} \approx 1.2$ and $m_{gen} \approx 0.6$. The maximum values of n_{gen} are approximately 2.2 for Acrylate A and 2.3 for Acrylate B. This represents a plausible spectrum for n_{gen} and indicates a purely homogenous chemical reaction as described before. The maximum values for m_{gen} are approximately 0.8 for Acrylate A and 0.9 for Acrylate B. As stated by Kamal,³⁰ $m_{gen} < 1$ is a common occurrence and represents a plausible value for the autocatalytic reaction order. In addition, the independence of the reaction order from the isothermal temperature as stated by Kamal³⁰ becomes apparent for both materials. Therefore, the chemical plausibility for the magnitude of the reaction orders can be confirmed. For n_{gen} , the above-

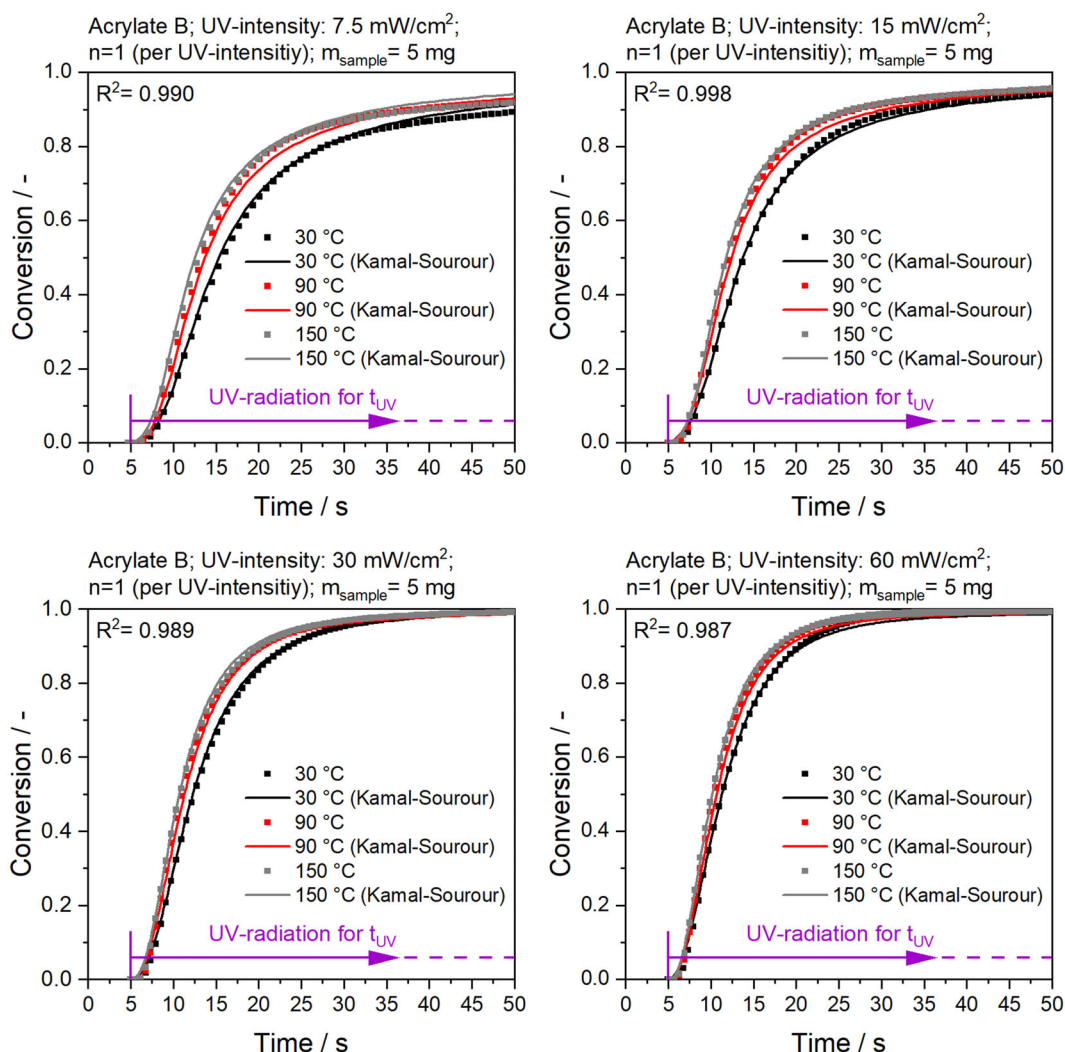


FIGURE 8 Clustered measurement analysis based on the Kamal–Sourour method described by Equation (11) of Acrylate B for UV intensities 7.5, 15, 30, and 60 mW/cm² as well as temperatures of 30, 90, and 150 °C.

described progression indicates a change from a near second-order reaction to a close to first- or pseudo-first-order reaction with increasing UV intensity. This constitutes the hypothesis, that the reaction mechanism shifts from a bimolecular reaction with collisions that contribute the energy to the reactant (second order) toward a more linear reaction with increased autocatalytic behavior and intermolecular collisions, which is the case for the majority of first-order reactions.

All in all, by comparing the Avrami method with the general Kamal–Sourour method, it can be concluded that the informational output from a chemical standpoint is higher for the Kamal–Sourour method than for the Avrami method. This is the case for both materials analyzed. Also, the coefficient of determination is significantly higher. The improved mathematical determination is mostly visible at the beginning and at the end of each reaction. Therefore, the

Kamal–Sourour method is selected for further clustered analysis. Especially the fluctuations in the values for k_1 and $k_2 \cdot K_{cat,gen}$ represent an aspect, which can potentially be decreased through clustered measurement analysis.

4.2 | Analysis of the influence of UV intensity and temperature with the Kamal–Sourour method based on clustered measurements

Based on the results from the single measurement analysis the Kamal–Sourour approach is selected for further clustered analysis. First, the UV-intensity-based clustering (compare Table 2) is analyzed. Accordingly, k_1 and k_2 of Equation (8) are substituted with Equation (9), resulting in Equation (11):

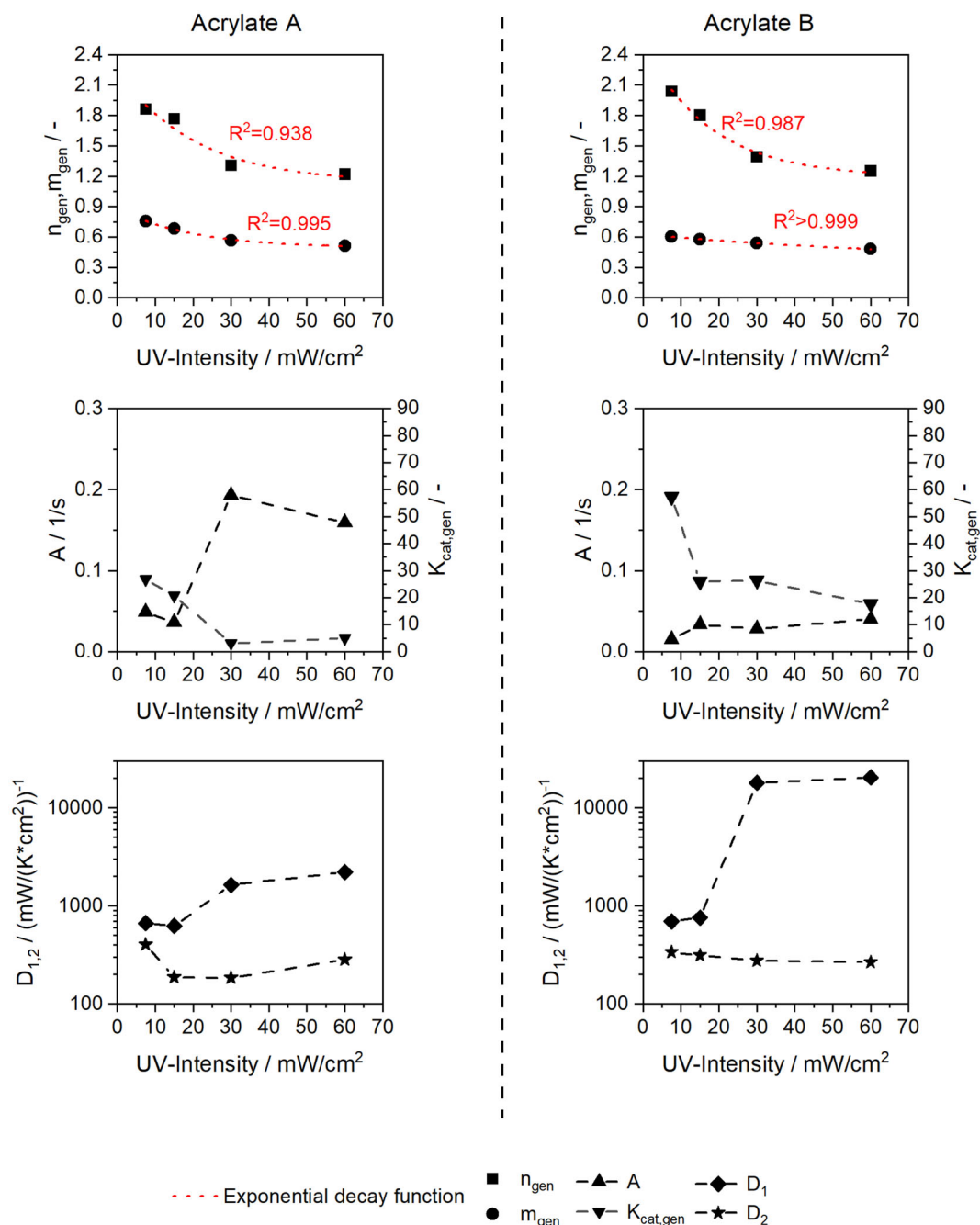


FIGURE 9 Dependency of the reaction orders n_{gen} and m_{gen} , the pre-exponential factors A and $K_{cat,gen}$ as well as the exponential factors D_1 and D_2 from the UV intensity for Acrylate A and Acrylate B (clustering based on the Kamal–Sourour method described using Equation (11))

$$\frac{d\alpha}{dt} = A \cdot e^{-D_1/T} \cdot (1 - \alpha)^{n_{gen}} + A \cdot K_{cat,gen} \cdot e^{-D_2/T} \cdot \alpha^{m_{gen}} (1 - \alpha)^{n_{gen}} \quad (11)$$

The equation demonstrates an independence of the reaction orders n_{gen} and m_{gen} from the temperature but a proportionality toward the UV intensity, which is congruent to the propositions by Kamal et al.³⁰ and correlates with the results from the single measurement analysis. Figures 7, 8

show the results for both materials based on Equation (11) compared with the originally measured data. For Acrylate A, the coefficients of determination R^2 show near identical values between 0.982 and 0.989. For Acrylate B, an outstanding R^2 of 0.998 is achieved for a UV intensity of 15 mW/cm². The other clusters also achieve values between 0.982 and 0.990, close to the range of Acrylate A.

The resulting kinetic parameters are depicted in Figure 9. For the reaction orders n_{gen} and m_{gen} , the curve

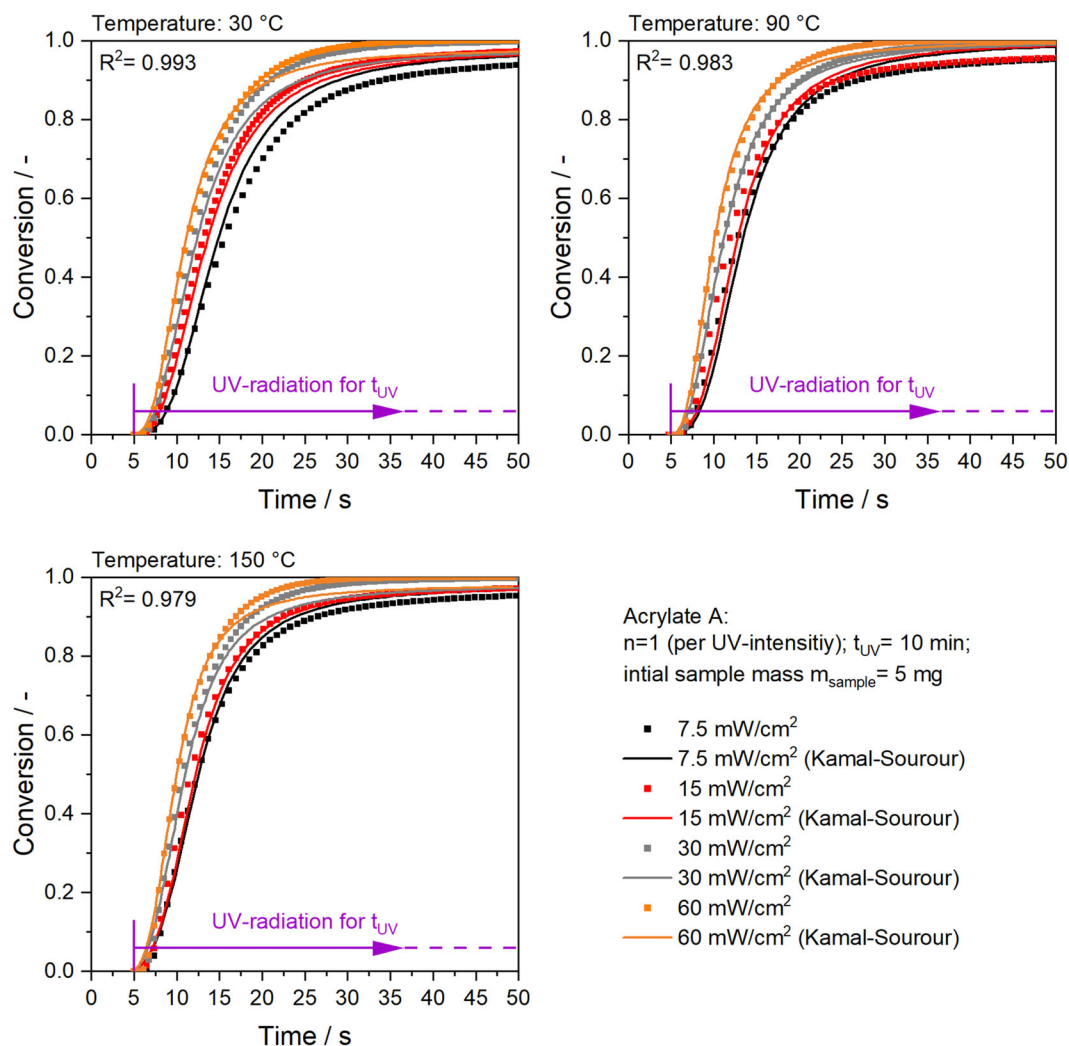


FIGURE 10 Clustered measurement analysis based on the Kamal–Sourour method described by Equation (12) of Acrylate A for UV intensities 7.5, 15, 30, and 60 mW/cm² as well as temperatures of 30, 90, and 150 °C.

progressions and the magnitudes are identical to the results of the single measurement analysis. Both parameters present themselves as exponential decay functions dependent on the UV intensity with decreasing values between approximately 2.1 and 1.2 for n_{gen} as well as 0.8 and 0.5 for m_{gen} . Curve fits of exponential decay functions are presented in Figure 9, which achieve R^2 values between 0.938 and above 0.999 for both materials analyzed.

In the case of the pre-exponential factors A and $K_{cat,gen}$ as well as the exponential factors D_1 and D_2 , the identification of an unambiguous mathematical progression is not possible. However, trends can be derived for all parameters. For increasing UV intensities, A also increases for both materials, with Acrylate A achieving higher values compared with Acrylate B. On the contrary, $K_{cat,gen}$ decreases with increasing UV intensities reminiscent of an exponential decay function. This potentially indicates a change in the reaction to a less

autocatalytically influenced reaction type with increasing UV intensities. The exponential factors D_1 and D_2 demonstrate contrary curve progressions and different magnitudes. D_1 achieves higher values compared with D_2 for both materials analyzed. Increasing UV intensities result in an increasing progression of D_1 and a decreasing or constant progression of D_2 .

The temperature-based clustering (compare Table 2) combines Equations (8) and (10) with Equation (12) below. The curve-fitting results and the progression of the kinetic parameters for different temperatures are presented in Figures 10–12, respectively.

$$\frac{d\alpha}{dt} = A \cdot e^{-D_1/I} \cdot (1 - \alpha)^{n_{gen}} + A \cdot K_{cat,gen} \cdot e^{-D_2/I} \cdot \alpha^{m_{gen}} (1 - \alpha)^{n_{gen}} \quad (12)$$

Figures 10, 11 illustrate the progression and accuracy of the curve-fitting results based on Equation (12).

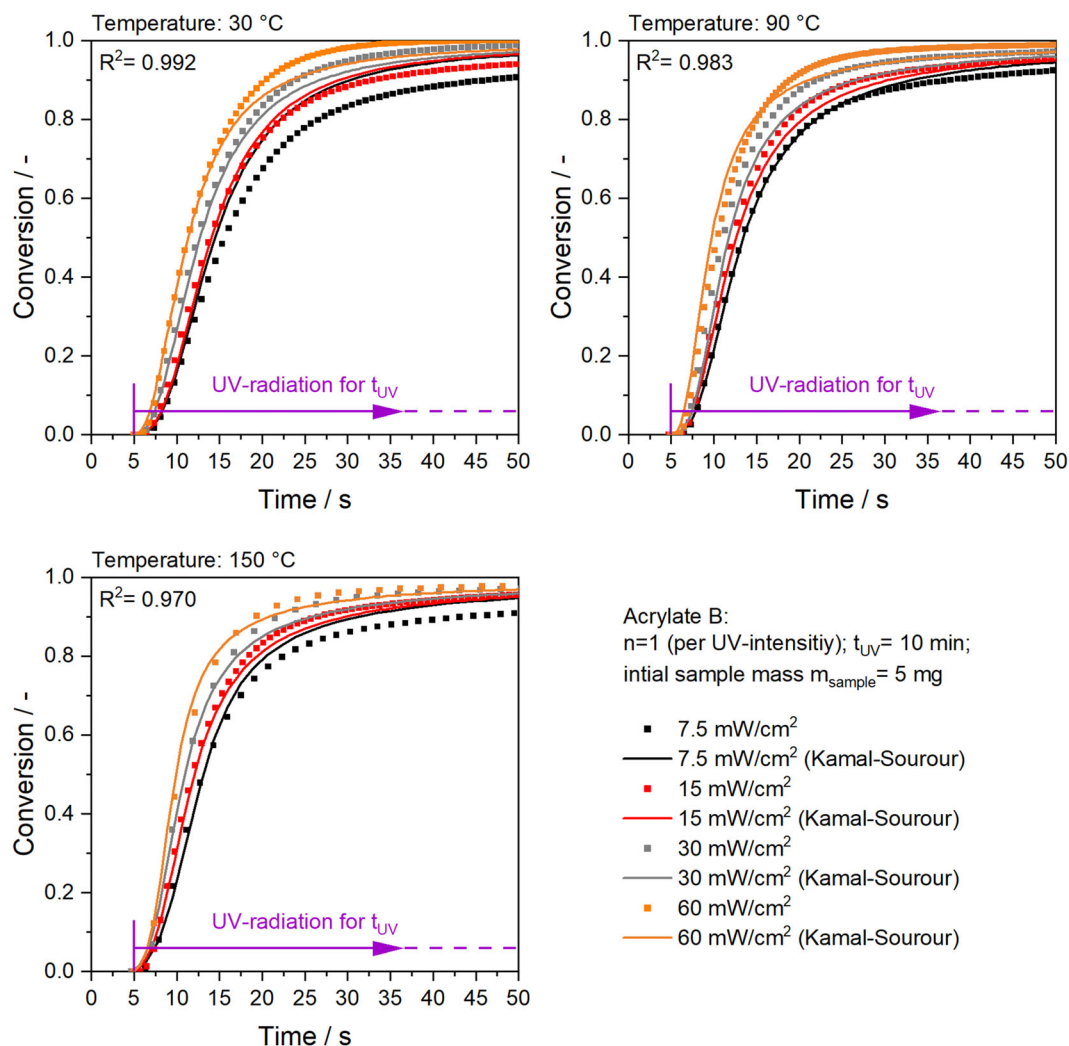


FIGURE 11 Clustered measurement analysis based on the Kamal–Sourour method described by Equation (12) of Acrylate B for UV intensities 7.5, 15, 30, and 60 mW/cm² as well as temperatures of 30, 90, and 150 °C.

Compared with UV-intensity clustering, the fit accuracy is slightly lower with coefficients of determination R^2 between 0.979 and 0.993 for Acrylate A as well as 0.970 and 0.992 for Acrylate B. The fit accuracy decreases for increasing temperatures, which potentially correlates with the increasing mass loss for higher temperatures. This mass loss is most likely correlated to evolving gases originating from the diacrylate monomers of both materials in a liquid state and was documented in detail in Reference [4]. The analysis of the kinetic parameters is illustrated in Figure 12. Contrary to the clustering based on Equation (11) and the results from single measurement analysis, the clustering based on Equation (12) neglects the dependency of the reaction orders n_{gen} and m_{gen} from the UV intensity. Instead, the dependence of the reaction orders is solely UV-based. However, both materials indicate an independence of n_{gen} and m_{gen} from the temperature, with constant values of $n_{gen} \approx 1.4$ and

$m_{gen} \approx 0.6$ for Acrylate A as well as $n_{gen} \approx 1.7$ and $m_{gen} \approx 0.6$ for Acrylate B. For n_{gen} of Acrylate B, only a slight increase is visible for increasing temperatures, which is neglected for the rest of this investigation. As discussed before, the independence of the reaction orders from the temperature is compliant with the descriptions of Kamal et al.³⁰ and correlates with the results from single measurement analysis. For all other kinetic parameters, a mathematical description can be performed with linear curve fits. For both materials, the pre-exponential factor A shows a linear decline with increasing temperatures, while $K_{cat,gen}$ shows a linear increase with increasing temperatures. This potentially indicates a change in the reaction to a more autocatalytically influenced reaction type with increasing temperatures. Acrylate B shows higher maximum values for both A and $K_{cat,gen}$ with steeper linear progressions. For both materials, linear fits are performed based on the A and $K_{cat,gen}$ which are

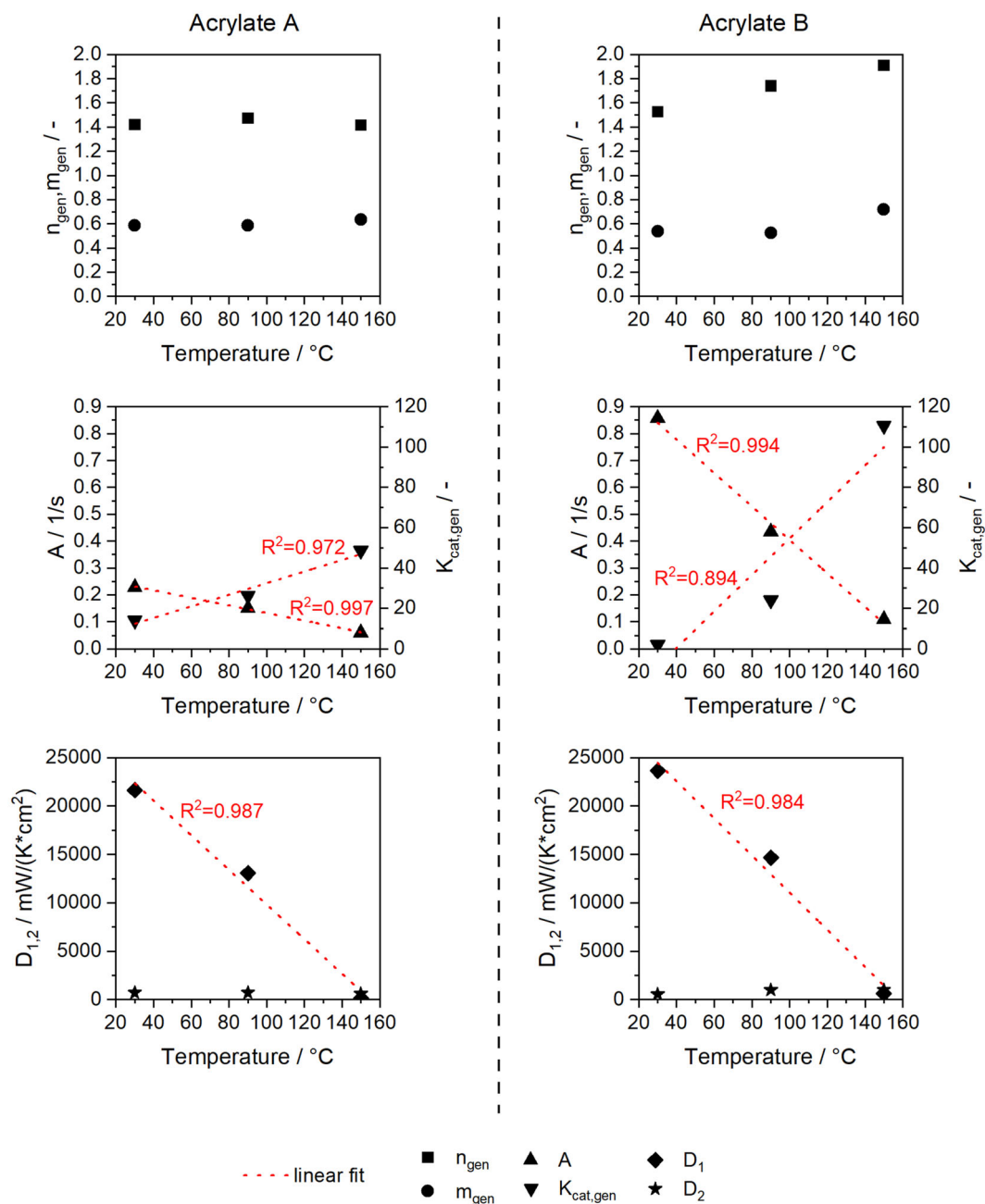


FIGURE 12 Dependency of the reaction orders n_{gen} and m_{gen} , the pre-exponential factors A and $K_{cat,gen}$ as well as the exponential factors D_1 and D_2 from different isothermal temperatures for Acrylate A and Acrylate B (clustering based on the Kamal-Sourour method described in Equation (12)).

illustrated in Figure 12. The fit accuracy for Acrylate A is comparably higher, with coefficients of determination R^2 of 0.997 and 0.972 for A and $K_{cat,gen}$, respectively, compared with 0.994 and 0.894 of Acrylate B. For the exponential factor D_1 , a linear decrease for increasing temperatures is visible for both materials with nearly identical slopes. In comparison, D_2 shows stable values for increasing temperatures. This potentially indicates that only one of the reaction paths is dependent on the temperature and that the reaction rate is lowered by

increasing temperatures, which is compliant to an increased movement of the polymer-building elements on a molecular level as stated by the collision theory by Trautz³⁹ and Lewis.⁴⁰

By comparing the kinetic models based on Equations (11) and (12), it is apparent that Equation (12) reaches a higher mathematical determination besides achieving a marginally lower fit accuracy. Also, the chemical plausibility of this approach is higher for being compliant with the temperature independence of the reaction

orders from the temperature as well as the accelerating impact of increasing temperatures on the reaction rate. Based on the model described through Equation (12), individual isothermal predictions regarding not-measured UV intensities can be performed, which is exemplified in Figure 1C for Acrylate A at UV intensities of 45 and 90 mW/cm² and a temperature of 90°C. Both predictions demonstrate a reasonable progression compared with the measured data. The linear progression of the fitting curves for different kinetic parameters however represents a debatable aspect, because it builds a mathematical function without any stagnation or natural end. In this case, the method based on Equation (11) presents a more realistic progression with high reminiscence exponential decay function for most kinetic parameters analyzed. Further measurements with a broader spectrum of UV intensities and the analysis of other materials are necessary to maximize reproducibility and solidify the results toward further mathematical dependencies. In retrospective of the target to use both materials for temperature-intensive AM applications, the kinetic model based on Equation (12) represents a viable method to predict the curing behavior for sufficient mechanical properties and optimize the processing time toward shortened production cycles and layer times. It is possible to predictively optimize the UV intensity and the isothermal temperature of the future process to meet production goals and minimize unwanted effects like thermal degradation while maintaining the desired level of curing.

5 | CONCLUSION

This investigation successfully demonstrated the evaluation, selection, and strategic progression of kinetic modeling procedures for UV-curable Acrylates of next-generation AM technologies. Based on UV-DSC measurements, different models were analyzed first based on single measurements and subsequently for clustered measurements. The kinetic models in their original state were selected based on the literature and the state-of-the-art. For single measurement analysis, the fit accuracy based on the average coefficient of determination R^2 showed acceptable results for most of the kinetic models selected. Best results were achieved using the Kamal–Sourour method and the Avrami method. Especially the sigmoidal aspect at the start and before entering the plateau region of the curing reaction is superiorly captured by the Kamal–Sourour method. Based on the high coefficients of determination, there is a strong endorsement for the theory of a combined autocatalytic and n -th order reaction. In case of the respective reaction orders, the Kamal–Sourour method demonstrated

proportionality with the UV intensity but independency from the isothermal temperature during curing. This is compliant with the propositions by Kamal et al.³⁰ and supports the hypothesis of decreasing reaction orders for both materials solely dependent on the UV intensity. In the case of the Avrami method, an increasing UV intensity respectively causes an increase in the reaction order. The progression is approximated to a limited growth function with stagnation at high UV intensities. This is contrary to the reaction orders of the Kamal–Sourour method. Here, the reaction orders approximately decrease exponentially with stagnation at higher UV intensities. Either progression is plausible since neither the increase nor the decrease progress infinitely and find a natural end by reaching a respective stagnation level. The magnitude of the reaction orders is in a plausible spectrum for both models. Eventually, the higher coefficients of determination compared with Avrami as well as the increased chemical plausibility and informational output led to the selection of the Kamal–Sourour method for subsequent modeling of the curing kinetics based on clustered measurements. Two different clustering strategies were analyzed: UV-intensity-based and temperature-based (compare Table 2 as well as Equations (11) and (12)). Both models comply with the aforementioned assumptions by Kamal et al., which state the temperature independence of the reaction order. In both cases, the reaction orders are within plausible magnitudes. The clustered measurement analysis based on Equation (11) demonstrates the exponential decay of the reaction orders for increasing UV intensities, which is compliant with the results of the single measurement analysis. Overall, the model based on Equation (12) reaches a higher mathematical determination for all kinetic parameters. Even isothermal predictions are possible for UV intensities that have not been measured yet. The calculated progressions showed reasonable results compared with the measured UV-DSC data. Further analysis shows that the kinetic parameters are either constant or follow a near-linear increase or decrease for increasing temperatures. In future investigations, further measurements and materials are necessary to maximize reproducibility and to solidify the results toward these mathematical dependencies. This represents the last steps toward a holistic approach for dynamic inclusion of the UV intensity and the temperatures to mathematically describe the curing behavior of acrylates for next-generation AM technologies. The kinetic models facilitate the predictive optimization of the process parameters to utilize a desired degree of cure within a temperature-intensive AM environment while limiting thermal decomposition and deterioration of the part properties.

ACKNOWLEDGMENTS

The authors gratefully acknowledge Deutsche Forschungsgemeinschaft (DFG, German Research Foundation) for funding in the framework of SFB 814 "Additive Manufacturing" TP B7. Open Access funding enabled and organized by Projekt DEAL.

DATA AVAILABILITY STATEMENT

The data that support the findings of this study are available on request from the corresponding author.

ORCID

Robert Setter  <https://orcid.org/0000-0003-2166-2794>

Natalie Rudolph  <https://orcid.org/0000-0003-2899-3422>

Katrin Wudy  <https://orcid.org/0000-0002-3384-4651>

REFERENCES

- Wudy K, Drummer D. Infiltration behavior of thermosets for use in a combined selective laser sintering process of polymers. *JOM*. 2019;71(3):920-927. doi:10.1007/s11837-018-3226-0
- Setter R, Riedel F, Peukert W, Schmidt J, Wudy K. Infiltration behavior of liquid thermosets in thermoplastic powders for additive manufacturing of polymer composite parts in a combined powder bed fusion process. *Polym Compos*. 2021;42(10):5265-5279. doi:10.1002/pc.26221
- Setter R, Stichel T, Schuffenhauer T, Kopp S-P, Roth S, Wudy K. *Additive Manufacturing of Multi-material Polymer Parts Within the Collaborative Research Center 814*. Springer International Publishing; 2021:142-152.
- Setter R, Schmölder S, Rudolph N, Moukhina E, Wudy K. Thermal stability and curing behavior of acrylate photopolymers for additive manufacturing. *Polym Eng Sci*. Published online May 22, 2023. doi:10.1002/pen.26355
- Bloh JZ. A holistic approach to model the kinetics of photocatalytic reactions. Original research. *Front Chem*. 2019;7.
- Redmann A, Oehlmann P, Scheffler T, Kagermeier L, Osswald TA. Thermal curing kinetics optimization of epoxy resin in Digital Light Synthesis. *Additive Manufacturing*. 2020;32:101018. doi:10.1016/j.addma.2019.101018
- Konuray O, Salla JM, Morancho JM, Fernández-Francos X, García-Alvarez M, Ramis X. Curing kinetics of acrylate-based and 3D printable IPNs. *Thermochim Acta*. 2020;692:178754. doi:10.1016/j.tca.2020.178754
- Bauer J, Izard AG, Zhang Y, Baldacchini T, Valdevit L. Thermal post-curing as an efficient strategy to eliminate process parameter sensitivity in the mechanical properties of two-photon polymerized materials. *Opt Express*. 2020;28(14):20362-20371. doi:10.1364/OE.395986
- Taki K. A simplified 2D numerical simulation of photopolymerization kinetics and oxygen diffusion-reaction for the continuous liquid interface production (CLIP) system. *Polymers*. 2020;12(4). doi:10.3390/polym12040875
- Kim YC, Hong S, Sun H, et al. UV-curing kinetics and performance development of in situ curable 3D printing materials. *Eur Polym J*. 2017;93:140-147. doi:10.1016/j.eurpolymj.2017.05.041
- Bachmann J, Gleis E, Schmölder S, Fruhmann G, Hinrichsen O. Photo-DSC method for liquid samples used in vat photopolymerization. *Anal Chim Acta*. 2021;1153:338268. doi:10.1016/j.aca.2021.338268
- Esposito Corcione C, Frigione M, Maffezzoli A, Malucelli G. Photo-DSC and real time-FT-IR kinetic study of a UV curable epoxy resin containing o-Boehmites. *Eur Polym J*. 2008;44(7):2010-2023. doi:10.1016/j.eurpolymj.2008.04.030
- Jiang F, Drummer D. Curing kinetic analysis of acrylate photopolymer for additive manufacturing by photo-DSC. *Polymers*. 2020;12(5). doi:10.3390/polym12051080
- Haines PJ, Reading M, Wilburn FW. Chapter 5 - Differential thermal analysis and differential scanning calorimetry. In: Brown ME, ed. *Handbook of Thermal Analysis and Calorimetry*. Elsevier Science B.V.; 1998:279-361.
- Galwey AK, Brown ME. Chapter 3 - Kinetic background to thermal analysis and calorimetry. In: Brown ME, ed. *Handbook of Thermal Analysis and Calorimetry*. Elsevier Science B.V.; 1998:147-224.
- Arrhenius S. Über die Reaktionsgeschwindigkeit bei der Inversion von Rohrzucker durch Säuren. *Z Phys Chem (N F)*. 1889;4U(1):226-248. doi:10.1515/zpch-1889-0416
- Avrami M. Kinetics of phase change. I General theory. *J Chem Phys*. 1939;7(12):1103-1112. doi:10.1063/1.1750380
- Murias P, Byczyński Ł, Maciejewski H, Galina H. A quantitative approach to dynamic and isothermal curing of an epoxy resin modified with oligomeric siloxanes. *J Therm Anal Calorim*. 2015;122(1):215-226. doi:10.1007/s10973-015-4703-0
- Xu W, Bao S, Shen S, Wang W, Hang G, He P. Differential scanning calorimetric study on the curing behavior of epoxy resin/diethylenetriamine/organic montmorillonite nanocomposite. *J Polym Sci B: Polym Phys*. 2003;41(4):378-386. doi:10.1002/polb.10365
- Freeman ES, Carroll B. The application of thermoanalytical techniques to reaction kinetics: the thermogravimetric evaluation of the kinetics of the decomposition of calcium oxalate monohydrate. *J Phys Chem*. 1958;62(4):394-397. doi:10.1021/j150562a003
- Sesták J, Satava V, Wendlandt WW. The study of heterogeneous processes by thermal analysis. *Thermochim Acta*. 1973;7(5):333. doi:10.1016/0040-6031(73)87019-4
- Criado JM, Dollimore D, Heal GR. A critical study of the suitability of the freeman and carroll method for the kinetic analysis of reactions of thermal decomposition of solids. *Thermochim Acta*. 1982;54(1):159-165. doi:10.1016/0040-6031(82)85075-2
- Jerez A. A modification to the Freeman and Carroll method for the analysis of the kinetics of non-isothermal processes. *J Therm Anal*. 1983;26(2):315-318. doi:10.1007/BF01913218
- Šesták J, Berggren G. Study of the kinetics of the mechanism of solid-state reactions at increasing temperatures. *Thermochim Acta*. 1971;3(1):1-12. doi:10.1016/0040-6031(71)85051-7
- Prout EG, Tompkins FC. The thermal decomposition of potassium permanganate. *Trans Faraday Soc*. 1944;40(0):488-498. doi:10.1039/TF9444000488
- Du S, Guo Z-S, Zhang B, Wu Z. Cure kinetics of epoxy resin used for advanced composites. *Polym Int*. 2004;53(9):1343-1347. doi:10.1002/pi.1533

27. Zhuqing Z, Wong CP. Modeling of the curing kinetics of no-flow underfill in flip-chip applications. *IEEE Trans Compon Packaging Technol.* 2004;27(2):383-390. doi:[10.1109/TCAPT.2004.828556](https://doi.org/10.1109/TCAPT.2004.828556)
28. Raja Pandiyan KR, Chakraborty S, Kundu G, Neogi S. Curing kinetics of medium reactive unsaturated polyester resin used for liquid composite molding process. *J Appl Polym Sci.* 2009; 114(4):2415-2420. doi:[10.1002/app.30720](https://doi.org/10.1002/app.30720)
29. Galukhin A, Nosov R, Taimova G, Nikolaev I, Islamov D, Vyazovkin S. Polymerization kinetics of adamantane-based dicyanate ester and thermal properties of resulting polymer. *React Funct Polym.* 2021;165:104956. doi:[10.1016/j.reactfunctpolym.2021.104956](https://doi.org/10.1016/j.reactfunctpolym.2021.104956)
30. Kamal MR. Thermoset characterization for moldability analysis. *Polym Eng Sci.* 1974;14(3):231-239. doi:[10.1002/pen.760140312](https://doi.org/10.1002/pen.760140312)
31. Vyazovkin S, Burnham AK, Favregeon L, et al. ICTAC Kinetics Committee recommendations for analysis of multi-step kinetics. *Thermochim Acta.* 2020;689:178597. doi:[10.1016/j.tca.2020.178597](https://doi.org/10.1016/j.tca.2020.178597)
32. Kenny JM. Determination of autocatalytic kinetic model parameters describing thermoset cure. Note. *J. Appl Polym Sci.* 1994;51(4):761-764. doi:[10.1002/app.1994.070510424](https://doi.org/10.1002/app.1994.070510424)
33. Kuppasamy RRP, Zade A, Kumar K. Time-temperature-cure process window of epoxy-vinyl ester resin for applications in liquid composite moulding processes. *Mater Today: Proc.* 2021; 39:1407-1411. doi:[10.1016/j.matpr.2020.05.048](https://doi.org/10.1016/j.matpr.2020.05.048)
34. Photocentric-Group. UV DLP Hard Safety Datasheet. 2022.
35. Photocentric-Group. UV DLP Firm Safety Datasheet. 2022.
36. Wang X, Schmidt F, Hanaor D, Kamm PH, Li S, Gurlo A. Additive manufacturing of ceramics from preceramic polymers: a versatile stereolithographic approach assisted by thiol-ene click chemistry. *Addit Manuf.* 2019;27:80-90. doi:[10.1016/j.addma.2019.02.012](https://doi.org/10.1016/j.addma.2019.02.012)
37. More JJ. Levenberg--Marquardt algorithm: implementation and theory. In: *Report Number: CONF-770636-1.* 1977.
38. Kutta W. Beitrag zur näherungsweise Integration totaler Differentialgleichungen. *Z Math Phys.* 1901;1901(46):435-453.
39. Trautz M. Das Gesetz der Reaktionsgeschwindigkeit und der Gleichgewichte in Gasen. Bestätigung der Additivität von Cv-3/2R. Neue Bestimmung der Integrationskonstanten und der Moleküldurchmesser. *Z Anorg Allg Chem.* 1916;96(1):1-28. doi:[10.1002/zaac.19160960102](https://doi.org/10.1002/zaac.19160960102)
40. Lewis WCM. XLI.—Studies in catalysis. Part IX. The calculation in absolute measure of velocity constants and equilibrium constants in gaseous systems. *J Chem Soc Trans.* 1918;113(0): 471-492. doi:[10.1039/CT9181300471](https://doi.org/10.1039/CT9181300471)

How to cite this article: Setter R, Schmölzer S, Rudolph N, Moukhina E, Wudy K. Modeling of the curing kinetics of acrylate photopolymers for additive manufacturing. *Polym Eng Sci.* 2023;63(7): 2149-2168. doi:[10.1002/pen.26353](https://doi.org/10.1002/pen.26353)